Original Research Article

International journal of spray and combustion dynamics

International Journal of Spray and Combustion Dynamics
2017, Vol. 9(4) 299–309

DOI: 10.1177/1756827717696326
journals.sagepub.com/home/scd
SAGE

Measurement and modeling of the generation and the transport of entropy waves in a model gas turbine combustor

Dominik Wassmer[1], Bruno Schuermans[2], Christian Oliver Paschereit[1] and Jonas P Moeck[3]

Abstract

Indirect combustion noise is caused by entropy spots that are accelerated at the first turbine stage. These so-called entropy waves originate from the equivalence ratio fluctuations in the air–fuel mixture upstream of the flame. As entropy waves propagate convectively through the combustion chamber, they are subject to diffusion and dispersion. Because of the inherent difficulty of accurately measuring the burned gas temperature with sufficient temporal resolution, experimental data of entropy waves are scarce. In this work, the transfer function between equivalence ratio fluctuations and entropy fluctuations is modeled by a linearized reactor model, and the transport of entropy waves is investigated based on a convection-diffusion model. Temperature fluctuations are measured by means of a novel measurement technique at different axial positions downstream of the premixed flame, which is forced by periodic fuel injection. Experiments with various flow velocities and excitation frequencies enable model validation over a wide range of parameters.

Keywords

Entropy wave, temperature measurement, equivalence ratio fluctuation, reactor model, transport model, dispersion

Date received: 5 September 2016; accepted: 3 February 2017

1. Introduction

Thermoacoustic phenomena are a major concern in the operation and development of gas turbine combustors, as they confine the operational window such that the reduction of emissions is substantially impeded. One mechanism contributing to the acoustics in a combustion chamber is indirect combustion noise. Non-isentropic temperature oscillations are generated by equivalence ratio fluctuations in the flame and advected to the first stage of the turbine. The flow is rapidly accelerated, and the incident entropy fluctuations are partly converted to acoustic waves, which are reflected back to the flame. This acoustic feedback might influence the thermoacoustic interaction between heat release rate fluctuations and the acoustic field in the combustion chamber, potentially leading to instabilities.[1–3]

This so-called entropy noise comprises two physical mechanisms. One is the generation of acoustic perturbations at the stator inlet downstream of the combustion chamber due to incident entropy waves. Analytically, this effect has been, amongst others, described by Bohn[4] and Marble and Candel.[5] It is still subject to detailed investigations dealing with more general and robust solutions for various boundary conditions and applied to realistic combustion systems.[6,7] Experiments were already conducted in 1976 by Zukoski and Auerbach,[8] employing a heating mesh to generate periodic temperature fluctuations. However, Bake et al.[9] were the first who were able to set up an experiment exhibiting an entropy wave with a considerably high amplitude in order to provide evidence of the associated generation of acoustic waves. In their work, the temperature fluctuation is introduced into a

[1]ISTA, HFI, Fluid Dynamics, TU Berlin, Germany
[2]GE Power, Baden, Switzerland
[3]ISTA, HFI, Combustion Dynamics, TU Berlin, Germany

Corresponding author:
Dominik Wassmer, ISTA, HFI, TU Berlin, Müller-Breslau-Str. 8, 10623, Berlin.
Email: dominik.wassmer@tu-berlin.de

duct flow also by means of a heating mesh, but their ''entropy wave generator'' achieved temperature amplitudes of up to 13 K instead of 1 K as in the case of Zukoski and Auerbach. A linear dependence between the amplitude of the entropy noise and the incident temperature amplitude has been found. Their work demonstrates the principal relevance of indirect combustion noise.

The other mechanisms, which have strong influence on whether indirect combustion noise is of relevance for a combustion system or whether it could possibly be neglected, are the generation and transport processes of entropy fluctuations. The formation process of entropy fluctuations has been investigated by Dowling and Stow.[10] They state that unsteadiness in entropy can only be caused by heat release rate fluctuations per unit mass of the fuel–air mixture. It therefore follows that entropy waves can only be generated by equivalence ratio fluctuations (and not by heat release rate fluctuations due to, e.g. flame surface area fluctuations). However, in a recent careful analysis, Strobio Chen et al.[11] have shown that this holds only under rather restrictive conditions. They resolve the controversy that arises when deriving the aforementioned corollary and they work out the assumptions that have to be made in order to neglect acoustic perturbations as cause for fluctuations in entropy. These are the compactness of the flame with respect to the acoustic wavelength and with respect to the convective wavelength of the equivalence ratio fluctuation, complete and adiabatic combustion, low Mach numbers, and the radial homogeneity of the flame front. Not all of these assumptions might hold true in real combustors but are regarded as acceptable for the experimental investigations in this work.

Eventually this leads to the same relation between the equivalence ratio fluctuations ϕ' and the associated entropy fluctuations s' downstream of the flame as found by Polifke et al.[1]

$$s' = c_p \frac{T'_{\text{hot}}}{\bar{T}_{\text{hot}}} = c_p \left(1 - \frac{\bar{T}_{\text{cold}}}{\bar{T}_{\text{hot}}}\right) \frac{\phi'}{\bar{\phi}} \tag{1}$$

where c_p denotes the specific heat capacity of air at constant pressure.

In order to obtain the response of the heat release rate fluctuation, which finally causes the unsteady entropy, to an equivalence ratio fluctuation, Lieuwen and Zinn[12] analyzed a well-stirred reactor model. They conclude that in the lean regime, the magnitude of the relative heat release rate fluctuations is approximately equal to the magnitude of the relative equivalence ratio fluctuations. Contrary to the acoustic perturbations, the assumption of the flame being compact with respect to the wavelength does not hold any more for advectively transported equivalence ratio fluctuations. Their approach accounts for different convective time delays due to the spatial distribution of the equivalence ratio fluctuations; however, only the phase angle of the heat release rate oscillation is affected, the magnitude is not attenuated.

Therefore, a distributed time lag model has been developed, which does not only account for the flame shape but also includes the effect of dispersion and diffusion on the transport of the equivalence ratio to the flame front.[13] This model is applicable for the transport of the equivalence ratio from the fuel injector to the flame front as well as for the propagation of the associated entropy spot downstream through the combustion chamber.

In turbulent flows with complex velocity fields, the effect of dispersion on the propagation of a scalar quantity has to be included. Sattelmayer[13] considered the spatial dispersion of a scalar field due to recirculation zones, the boundary layer, and turbulent diffusion present in a gas turbine combustor. A transfer function, describing the change of amplitude and phase of a scalar depending on an average convective time delay and a time parameter, representing the spatial distribution of the time delays, is derived. The latter accounts for dispersion, and the ratio between the average delay time and the dispersive time dictates the strength of the amplitude decay for increasing oscillation frequencies. Based on his analysis, Sattelmayer[13] concluded that due to dispersion, entropy waves have no destabilizing effect on the combustor, even for low frequencies. Modifications of that model, introducing a Gaussian rather than a rectangular time delay distribution, can be found in Polifke et al.[14] and Schuermans et al.[15]

Employing a Gaussian time delay distribution, Morgans et al.[16] came to a different conclusion. They found that for typical gas turbine combustor geometries and characteristic flow fields, and for low frequencies, the entropy fluctuations survive the advection process and reach the turbine inlet with considerable amplitude. Goh and Morgans[17] introduced an additional factor, representing dissipative effects. Variation of this dissipative factor and the dispersion time allows their model to predict the thermoacoustic stability behavior of the combustion system.

All these aforementioned models are based on the analytical considerations and lack a profound experimental validation.[18] In this work, these missing experimental data are presented and compared with the analytical models.

2. Dynamic temperature measurement

Unsteady temperature measurements in combustor environments are inherently difficult. This has significantly impeded detailed investigations of the

propagation of entropy waves in the past. In order to study entropy waves under the harsh and high-temperature conditions in gas turbine combustors, a time-of-flight-based temperature measurement method has been developed. Other technical applications of time-of-flight approaches in the field of gas turbines can be found, amongst others, in Kleppe et al.,[19] DeSilva et al.,[20] or Shen et al.[21]

2.1. Time-of-flight approach

In this work, active pyrometry is employed, where an acoustic source is actively triggered. Two electrodes are installed close to the combustor wall in the combustion rig downstream of the flame. The electrodes provide an electrical discharge, which produces a very short acoustic pulse of less than 50 µs duration. This acoustic pulse is detected by means of seven 1/4 inch microphones mounted at the same axial position along the circumference. The electrodes are embedded into a ceramic adapter to prevent unintended conduction with the rig; a cross-sectional view of the setup is depicted in Figure 1. Based on the different arrival times of the acoustic signal at the microphones, the line integral of the inverse speed of sound along the acoustic paths can be determined. Assuming a constant ratio of specific heats γ, the temperature at the axial measurement plane is given as

$$T = c^2 \frac{M}{R\gamma} \tag{2}$$

where it has been assumed that the speed of sound, c, is constant over the cross section. R is the universal gas constant and M the molar mass. Each acoustic pulse excitation provides a temperature measurement over a time scale that corresponds to the spark duration plus the acoustic propagation time over the combustor cross section. This time scale is of the order of 100 µs and is short compared to the relevant frequency range of at most a few hundred Hertz. In a first step, this measurement technique assumes plane entropy waves, which means that the cross-sectional temperature distribution is homogeneous.

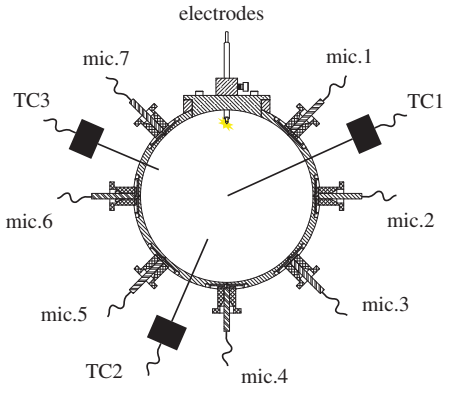

Figure 1. Principal setup of the time-of-flight measurement technique at the combustion rig; seven microphones and three thermocouples are installed around the circumference, at one axial location.

A crucial characteristic of the acoustic pulse generated by a spark discharge is its high frequency content above 20 kHz. This allows high-pass filtering of the microphone signals, which enables the threshold detection of the arrival of the very first acoustic pressure maximum, even under very noisy conditions as present in a gas turbine combustor. By means of a trigger signal associated with the entropy wave (e.g. OH*-chemiluminescence intensity, microphone signal or, as used in this work, the trigger pulse for the valve, which is forcing the fuel supply oscillations), phase averaging allows an arbitrary phase resolution of the oscillation cycle.

A robust method to reconstruct the temperature distribution within one period of oscillation is found by employing a singular value decomposition.[22] Here, knowledge about the distances between the origin of the spark discharge and the microphones is not required. Further information on the measurement technique and its validation, including a detailed description of the application of the singular value decomposition, can be found in Wassmer et al.[23]

A phantom study, which allows to analytically obtain the arrival times based on an artificial radial temperature profile, reveals very good agreement between the amplitude of the fluctuation of the imposed cross-sectionally-averaged temperature and the temperature amplitude extracted by means of the singular value decomposition. An error of less than 5% is found even for radially nonhomogeneous fluctuation amplitudes. The input temperature profile has been measured by means of a type-S thermocouple. The fact that the temperature obtained from the line integrated inverse speed of sound corresponds well to the cross-sectionally-averaged temperature stems from the favorable spatial distribution of the acoustic paths in the measurement setup. Thus, based on this temperature extraction technique, we measure the temperature which is relevant for the generation of indirect combustion noise.

2.2. Combustion rig setup

The novel measurement technique, as described above, is implemented at an atmospheric combustion rig at TU Berlin (see Figure 2). A lean, premixed, and swirl-stabilized natural gas flame is operated in a 200 mm diameter quartz tube followed by a water-cooled exhaust duct of the same diameter, which at the

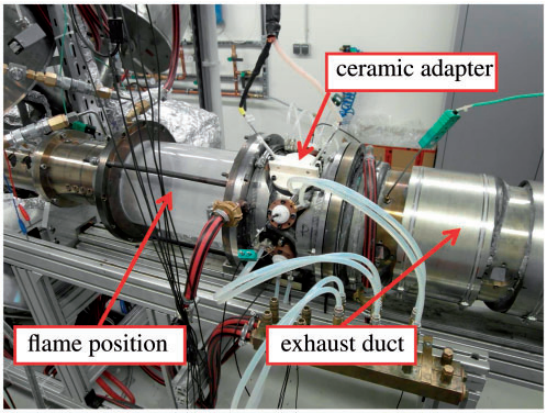

Figure 2. Measurement segment with ceramic adapter and water-cooled microphones along the circumference.

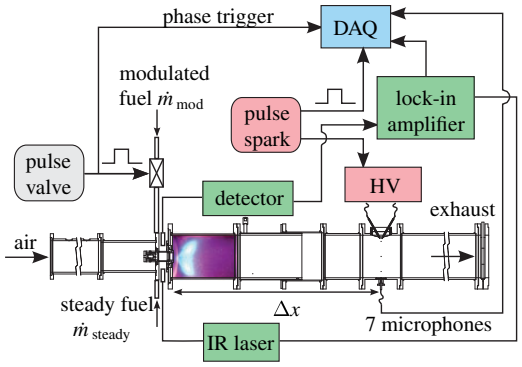

Figure 3. Schematic of the combustion chamber setup.

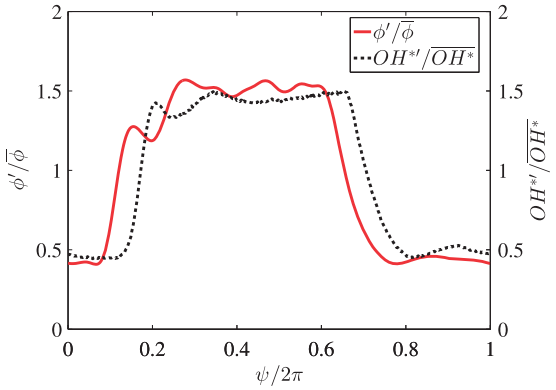

Figure 4. Relative fluctuations of the equivalence ratio and the OH*-intensity over one period of fuel modulation at $f_v = 20$ Hz.

downstream end is terminated by an orifice. A principle schematic of the rig is depicted in Figure 3. The burner is fed by two fuel supply lines. One is used for a steady fuel mass flow whereas the fuel mass flow through the second fuel line is modulated via an injection valve in order to generate well-defined equivalence ratio fluctuations.

Optical access via a transparent mixing tube between the swirler and the burner front plate allows for the detection of equivalence ratio fluctuations by means of tunable diode laser absorption spectroscopy (TDLAS).[24,25] OH* intensity fluctuations are simultaneously measured in the combustion zone via a photomultiplier equipped with a 308 nm band-pass filter. Due to a modular setup of the rig, the measurement segment, where the electrodes and seven microphones are mounted, can be placed at various axial positions downstream of the flame. The microphones are cased in water-cooled holders and evenly distributed along the circumference at angles from 45° to 315° with respect to the electrodes. The mean temperature at the measurement plane is detected via three type-K thermocouples located between the microphones. Their penetration depths range from the center of the rig to a position close to the combustor wall (see Figure 1). This allows an estimation of the radial static temperature field and consequently of the average static temperature at the measurement plane.

The swirl-stabilized flame is operated in a lean regime, the mean equivalence ratio $\bar{\phi}$ is kept constant at $\bar{\phi} = 0.6$. A share of 25% of the total fuel mass flow is modulated by the valve, which switches from open to close with a duty-cycle of 50% for all frequencies. The remaining 75% of the fuel mass flow is bypassed and injected together with the modulated fuel into the swirler upstream of the mixing tube. The TDLAS measurement of the methane concentration in the center of the mixing tube reveals that the equivalence ratio fluctuation ϕ' is not significantly damped by the mixing with the steady fuel mass flow and the air mass flow in the swirler. In Figure 4, the phase-averaged time trace of the TDLAS measurement is plotted over one period of valve excitation at a frequency of 20 Hz (solid line). The characteristic pulse shape imprinted by the injection valve is clearly visible; the same holds for the global OH* intensity measured at the flame position (dotted line).

The spark discharge between the electrodes is generated via a high-voltage coil driven by a MOSFET, which is triggered by a rectangular pulse signal. The repetition frequency of the pulse is chosen such that a period of an entropy fluctuation is sampled by a sufficient number of distinct phase angles. Due to the MOSFETs limits and the required pulse width for a proper electric discharge, the repetition frequency of the spark is limited to a maximum of 50 Hz. A sawtooth signal triggered by the pulse for the valve allows an accurate phase allocation of each spark discharge. The time delay between the switch of the MOSFET and the actual ignition of the spark is, amongst other

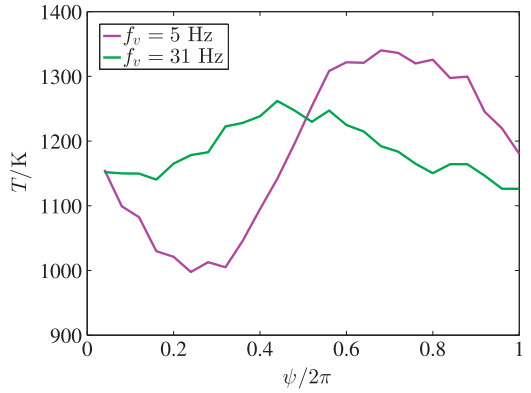

Figure 5. Time-of-flight-based temperature measurement over one period of fuel pulse excitation of 5 Hz (purple) and 31 Hz (green).

parameters, a function of temperature. Defining the traveling time of the acoustic pulse as the time span between the switch of the MOSFET and the arrival of the first acoustic pressure maximum at the microphone would hence be inherently error prone. However, a very short electromagnetic pulse (<1 µs) is transmitted with speed of light from the discharge location to the microphones. This disturbance signal is detected by the microphones prior to the pressure wave and is used as time stamp zero, where the acoustic signal is generated.

2.3. Combustion rig measurements

According to the procedure described in the theory section, one period of entropy oscillation is sampled with 31 evenly spaced phase angles. In Figure 5, temperature fluctuations are exemplarily shown for two different frequencies. The amplitude and the phase of the fluctuations are identified by calculating the Fourier coefficient corresponding to the excitation frequency. To compensate for irregularities, e.g. the occasional three-dimensional displacement of the spark discharges, which results in different spatial origins of the acoustic pulse signal, the arrival times are phase averaged over a sufficient number of ignitions.

The three main parameters that have been varied in this investigation are the excitation frequency f_v of the fuel valve, the bulk flow velocity $\bar{u}$ in the rig, and the axial location Δx of the measurement plane, where the entropy wave is measured. An overview of the distances between burner inlet plate and measurement plane Δx and the associated bulk flow velocities $\bar{u} = \dot{m}/\rho/S$, with S denoting the cross-section area of the exhaust duct, is given in Table 1. The reduction in velocity for locations further downstream originates from the decrease in mean temperature due to the cooling of the combustor walls.

Table 1. Measurement parameters.

	$\bar{u}$/m/ s		
Δx/ m	$\dot{m} = 140$ kg/h	$\dot{m} = 180$ kg/h	$\dot{m} = 220$ kg/h
0.400	4.3	5.8	7.2
0.580	4.2	5.6	7.0
0.695	4.1	5.4	6.8
0.780	4.0	5.3	6.6
0.850	3.9	5.3	6.6
0.950	3.9	5.2	6.5

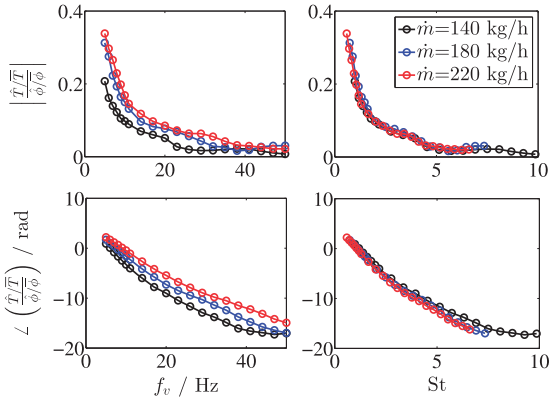

Figure 6. Absolute value (top row) and phase (bottom row) of the transfer function between the normalized temperature fluctuations and the normalized equivalence ratio fluctuations at $\Delta x = 0.78$ m; plotted over frequency (left column) and the Strouhal number (right column).

Based on these parameters, a dimensionless Strouhal number St can be defined as

$$St = \frac{f_v \Delta x}{\bar{u}} \tag{3}$$

which represents the ratio between the length scale Δx and the convective wave length $\lambda_c = \bar{u}/f_v$. In Figure 6, the temperature amplitude T', scaled with the static mean temperature $\bar{T}$ and normalized with the relative equivalence ratio fluctuation $\phi'/\bar{\phi}$, is plotted for three different mass flows of air, measured at one axial location $\Delta x = 0.78$ m. As the relative fluctuation of the equivalence ratio is the same for all frequencies, it can be seen that the relative amplitude of the temperature fluctuation is larger for higher mass flows. This can be explained by a shorter residence time of the temperature fluctuation between its formation at the flame and the measurement plane. On the right-hand side of Figure 6, the same data are plotted with respect to the Strouhal number St. The very distinct match

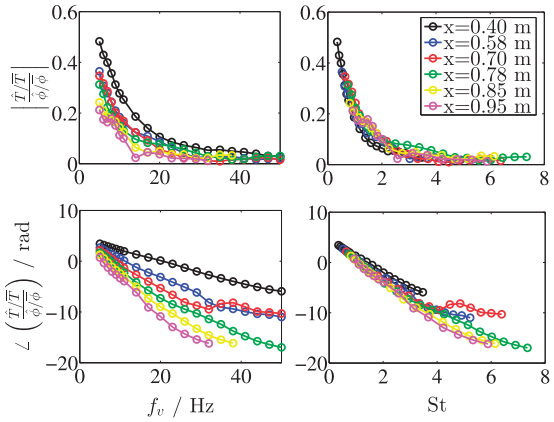

Figure 7. Absolute value (top row) and phase (bottom row) of the transfer function between the normalized temperature fluctuations and the normalized equivalence ratio fluctuations for $\dot{m} = 180$ kg/h; plotted over frequency (left column) and the Strouhal number (right column).

between the absolute values as well as the phases shows that the propagation of the entropy wave adheres well to Strouhal number scaling.

A similar effect is observed for the dependence of the relative temperature fluctuation on the convective length Δx, the distance between the entropy wave's origin at the flame and the measurement plane. In Figure 7, the modulus and the phase angle of the relative temperature amplitude is plotted for one air mass flow and six different axial locations. The amplitudes of the normalized temperature fluctuations decrease for further downstream locations since the entropy wave is subject to diffusion and dispersion when being advected through the duct. A good match of the absolute values as well as the phase is found when relating the relative temperature fluctuation to the Strouhal number, where again Δx is defined as the distance between the measurement plane and the burner inlet plane.

The broad variation of parameters, such as fuel excitation frequencies, flow velocities, and axial measurement locations build a profound base for modeling the generation and the transport effects of entropy waves. This is presented in the following.

3. Modeling approaches

To analytically describe the generation and transport of entropy waves, two separate models are derived. One model evaluates the transfer function between the equivalence ratio fluctuations and the generated temperature fluctuations, and a one-dimensional transport model accounts for the convective transport of the temperature spot in axial direction. Note that in the following, the focus lies on temperature fluctuations, as the temperature is the physical quantity that is measured. According to equation (1), for the assumption of a constant ratio of specific heats, γ, entropy fluctuations are directly related to relative temperature fluctuations.

3.1. Reactor model

The flame zone is in a first step considered as a homogeneous reactor of volume V_r. A cold air mass flow $\dot{m}_1$ is entering together with the fuel mass flow $\dot{m}_f$, and a hot exhaust gas mass flow $\dot{m}_2$ leaves the reactor at its downstream end. We assume ideal gas, isobaric combustion, and a high Damköhler number for the well-stirred homogeneous reactor. The latter assumption is valid as the time scales of the relevant equivalence ratio fluctuations are much larger than those of the reaction rate.[26] It is also assumed that there is no unsteady entropy upstream of the flame ($s'_1 = 0$). The energy balance for the reactor writes

$$\dot{m}_1 c_{p1} T_1 + Q = \dot{m}_2 c_{p2} T_2 \tag{4}$$

with the heat release rate $Q = \dot{m}_f h_f$, where h_f denotes the heat release per unit mass of fuel. Assuming a constant specific heat capacity c_p ($c_{p1} = c_{p2}$) and that the fuel mass flow is much smaller than the air mass flow ($\dot{m}_f/\dot{m}_1 \ll 1$), leads to $Q = \dot{m}_1 c_p \Delta T$ as an expression for the heat release rate. $\Delta T = T_2 - T_1$ represents the temperature difference from the cold state upstream of the flame to the combustion temperature.

We are now interested in the response of the system to a perturbation in the equivalence ratio, which occurs due to an imperfect mixing of fuel and air or, in our case, due to the fuel valve modulation in the experiments. It is assumed that the perturbations, denoted with $()'$, are sufficiently small, which justifies linearization around a mean value, denoted by $\overline{()}$. Linearization of equation (4) yields an expression for the fluctuating heat release rate

$$Q' = S\bar{\rho}_2 \bar{u}_2 \bar{T}_2 c_p \left(\frac{\rho'_2}{\bar{\rho}_2} + \frac{u'_2}{\bar{u}_2} + \frac{T'_2}{\bar{T}_2} \right) \tag{5}$$

where S denotes the cross-sectional area of the combustion chamber. Here, the effect of upstream velocity fluctuations on downstream entropy fluctuations is neglected; we only consider the effect of heat release rate fluctuations per unit mass of mixture on the quantities within the reactor zone. Therefore, the heat release rate fluctuation in equation (5) corresponds to the nonisentropic part of the total heat release rate fluctuation Q'_{tot} with $Q' = Q'_{\mathrm{tot}} - \bar{\rho}_2 c_p \Delta T u'_1$.[10]

The relative equivalence ratio fluctuations are of the order of the relative velocity fluctuations upstream of the flame ($\phi'/\bar{\phi} = \mathcal{O}(u'_1/\bar{u}_1)$) and the relative

temperature fluctuations downstream of the flame are in turn of the order of the relative equivalence ratio fluctuations ($T_2'/\bar{T}_2 = \mathcal{O}(\phi'/\bar{\phi})$). As for low Mach numbers the relative pressure fluctuations are much smaller than the relative velocity fluctuations ($p'/\bar{p} \ll u'/\bar{u}$), the linearized state equation for a perfect gas leads to

$$\frac{\rho_2'}{\bar{\rho}_2} = -\frac{T_2'}{\bar{T}_2} \tag{6}$$

By combining equations (6) and (5), and dividing by $\bar{Q} = \dot{m}_1 c_p \Delta T$, we obtain the relation between relative acoustic velocity fluctuations in the reactor and the unsteady heat release rate as

$$\frac{u_2'}{\bar{u}_2} = \frac{Q'}{\bar{Q}}\frac{\Delta T}{\bar{T}_2} \tag{7}$$

We further apply linearization to the mass conservation equation and obtain the following expression for the time derivative of the density ρ_2 within the reactor volume V_r

$$\frac{V_r}{\bar{\rho}_2 \bar{u}_2 S}\frac{\partial \rho_2}{\partial t} = -\frac{\rho_2'}{\bar{\rho}_2} - \frac{u_2'}{\bar{u}_2} \tag{8}$$

Employing equations (6) and (7), the normalized temperature fluctuation at the reactor exit is obtained as

$$\frac{T_2'}{\bar{T}_2} = \frac{V_r}{\bar{\rho}_2 \bar{u}_2 S}\frac{\partial \rho_2}{\partial t} + \frac{Q'}{\bar{Q}}\frac{\Delta T}{\bar{T}_2} \tag{9}$$

According to equation (6), the relative density fluctuation can be replaced by the negative relative temperature fluctuation. Using the proportionality between equivalence ratio and heat release rate, finally an expression for the transfer function between normalized temperature fluctuations and the associated equivalence ratio fluctuations is obtained in frequency domain

$$\hat{H}_r(\omega) = \frac{\hat{T}_2/\Delta T}{\hat{\phi}/\bar{\phi}} = \frac{1}{\frac{V_r}{\bar{u}_2 S} i\omega + 1} \tag{10}$$

with the angular frequency $\omega = 2\pi f$. $\widehat{()}$ denotes a fluctuating quantity in frequency domain. Equation (10) corresponds to a first-order low pass, a similar response was also found by Karimi et al.[27] who studied the frequency dependence of entropy generation due to acoustic and entropic excitation in a one-dimensional non-diffusive flow. They considered cases with steady as well as unsteady head addition into the flow and derived a formulation for a corner frequency of the generated entropy waves. By introducing a Strouhal number $St_r = (fL_f)/\bar{u}_r$, with L_f representing the reactor length (of the order of the flame length) and $\bar{u}_r$ denoting the mean flow velocity within the reactor, equation (10) reads

$$\hat{H}_r(St_r) = \frac{1}{i2\pi St_r + 1} \tag{11}$$

For $St_r = 1$ the reactor length is equivalent to the convective wavelength $\lambda_c = \bar{u}_r/f$, which corresponds to the idea of the corner frequency proposed by Karimi et al.[27] They state that the generation of entropic disturbances becomes small if "the entropic disturbance views a homogeneous region", which is the case for convective wavelengths of the equivalence ratio fluctuations that are smaller than the flame length. The ratio $L_f/\bar{u}_r$ that is contained in the Strouhal number can also be considered as a reactor residence time τ_r, which corresponds to the average time span a gas element remains inside the reactor.

For the validation of the reactor model, measured temperature fluctuations very close to the reactor are required, as transport losses are not considered in this model. To account also for the attenuation of the temperature fluctuations due to diffusion and dispersion downstream of the reactor zone, a separate transport model is derived in the following section.

3.2. Transport model

The transport of entropy waves has analytically been investigated by Morgans et al.[16] Dispersion is found to be the governing mechanism for the damping of entropy waves that are advected by a fully developed turbulent duct flow. Their entropy transport model, however, requires knowledge of the radial velocity field. As we did not assess the radial profile of the axial velocity in this study, a transport model is employed which contains an effective diffusivity to account for dispersive effects. The transport of the temperature fluctuations is then modeled as a one-dimensional convection-diffusion process[28]

$$\frac{\partial T'}{\partial t} + u\frac{\partial T'}{\partial x} - \alpha_{\text{eff}}\frac{\partial^2 T'}{\partial x^2} = 0 \tag{12}$$

α_{eff} is an effective diffusivity that models the effects of turbulent diffusion and dispersion. The idea to represent dispersive mechanisms by an effective diffusivity is based on an investigation by Taylor.[29] He found that with this formulation the evolution of an area-averaged passive scalar can be described even in the presence of a nonuniform flow field. Based on equation (12), a transfer function $\hat{H}_t(\omega) = \hat{T}(\omega, l_t)/\hat{T}(\omega, 0)$ mapping

fluctuations at $x = x_i$ to $x = x_j$ can be derived in frequency domain as

$$\hat{H}_t(St_t) = \exp\left(\frac{1}{2}Pe\left(1 - \sqrt{1 + i2\pi St_t \frac{4}{Pe}}\right)\right) \quad (13)$$

The Peclet-number Pe represents the ratio between a diffusion time scale $\tau_d = \Delta x_{ij}^2/\alpha_{\text{eff}}$ and a convective time scale $\tau_c = \Delta x_{ij}/\bar{u}$. Here, the transport Strouhal number St_t is defined as $St_t = (f\Delta x_{ij})/\bar{u}$ and can be interpreted as the ratio between the transport distance Δx_{ij} and the convective wavelength $\lambda_c = \bar{u}/f$ of the temperature fluctuation. In this investigation, the Strouhal number is fixed by the known transport length Δx_{ij} and the bulk flow velocity $\bar{u}$, whereas the effective diffusivity $\alpha_{\text{eff}} = \bar{u}\Delta x_{ij}/Pe$ (or the Peclet number Pe) needs to be fit to the measurements.

In Figure 8, the transport transfer function is depicted for different values of Pe. It can be seen that the magnitude of the transfer function at a particular frequency does not monotonically decrease for decreasing Peclet numbers. For some frequencies, the magnitude of the transport transfer function increases again if the Peclet number falls below a certain value; for the case shown in Figure 8, this value lies between $Pe = 1$ and $Pe = 10$.

For high Peclet numbers, when convection dominates over diffusion, equation (13) can be expressed as

$$\hat{H}_t(St_t) = e^{-i2\pi St_t} e^{-4\pi^2 St_t^2 Pe^{-1}} \quad (14)$$

The first exponential term represents a loss-free convective time delay, whereas the second exponential term accounts for a decay of magnitude for an increasing Strouhal number St_t and a decreasing Peclet number Pe. This representation is also found in Schuermans et al.,[15] where it is derived as the frequency response of the equivalence ratio in the flame to a perturbation at the fuel injector.

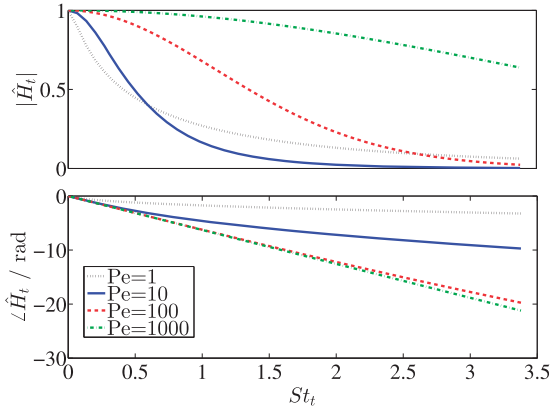

Figure 8. Absolute value (top) and phase (bottom) of the modeled transport transfer function $\hat{H}_t$ for different values of the Peclet number.

4. Modeling results

To validate the well-stirred reactor approach derived in the preceding section, the model is fit to the measured temperature fluctuations at the measurement plane that is closest to the flame ($\Delta x = 0.4\,\text{m}$). This is valid, as experimental flow field investigations have shown that the recirculation zone of the strongly swirled flow extends beyond the flame and approximately reaches this first measurement plane.

In Figure 9, the geometrical parameters of the model are displayed. Δx_i represents the distance between the combustor inlet plane and the measurement plane; L_f denotes the estimated flame length, which corresponds to the heat release zone. The only parameter in the reactor model (equation (11)) is the reactor residence time τ_r, which hence is subject to optimization. The temperatures T_1 and T_2 are estimated from thermocouple measurements. In order to account for the distance between the flame location and the measurement plane, $\hat{H}_r$ is multiplied by a convective time delay $e^{-i\omega(\Delta x_1 - L_f)/\tilde{u}_r}$. The reactor velocity $\tilde{u}_r$ is obtained from the phase relation between the measured temperature fluctuation at the measurement plane and the measured global OH*-chemiluminescence intensity at the flame location. Due to the short distance between flame and first measurement plane, loss-free convection is assumed.

In Figure 10, the measured and modeled absolute values and phase angles of the transfer functions between the relative temperature fluctuation at $\Delta x = 0.4\,\text{m}$ and the equivalence ratio fluctuations are depicted for two air mass flows, $\dot{m} = 140\,\text{kg/h}$ and $\dot{m} = 220\,\text{kg/h}$. A good match between modeled and measured magnitudes and phases is observed.

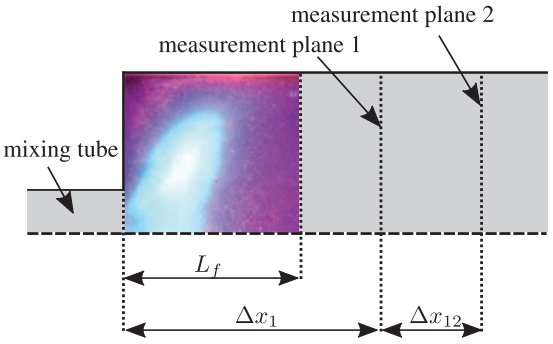

Figure 9. Display of model parameters and measurement planes.

The corresponding values of τ_r, resulting from the fitted model, are shown in Table 2 in the second column for all three mass flows. As was to be expected, the reactor residence time decreases for higher flow velocities. Based on the reactor residence times τ_r, an average reactor velocity $\bar{u}_r = \Delta x_1/\tau_r$ can be defined (see column 3 in Table 2). The good correspondence between $\bar{u}_r$ and $\tilde{u}_r$ suggests that the reactor model reproduces the measured temperature fluctuations in a physically meaningful way (compare column 3 and 4 in Table 2).

For the analysis of the transport model, we first look at the corresponding measurement results. Transfer functions between the normalized temperature fluctuations at the various axial measurement planes are evaluated. In Figure 11, the measured transport transfer functions (symbols) for five selected distances Δx_{ij} are plotted with respect to the transport Strouhal number $St_t = f\Delta x_{ij}/\bar{u}$, where Δx_{ij} denotes the distance between two measurement planes $|\Delta x_j - \Delta x_i|$.

A distinct decay of the transport transfer function for increasing Strouhal numbers is obtained. This is expected since for longer convective lengths as well as for higher frequencies the temperature waves are stronger affected by dispersion and diffusion. The relatively strong deviations of some values, e.g. Δx_{25}, might partly be explained by the errors of the dynamic temperature measurement technique, which have a greater impact for smaller distances between the measurement planes. Note that the measurements at each axial position were performed at different days, as the shift of the axial measurement plane requires cooling down of the combustion rig. The very good match of the phase angles, however, indicates that the estimation of the phase relation between two measurements is not influenced by these errors.

$\hat{H}_t$, as introduced in equation (13), is fit to the measured data in Figure 11 (solid lines). For this purpose, the Peclet number is optimized such that the absolute values as well as the phase angles of the transport transfer functions match the measurement. For the Peclet number, a value of $Pe = 30$ is found, this corresponds to effective diffusivities in the range of $\alpha_{\text{eff}} = 0.06\,\text{m}^2/\text{s}$ and $\alpha_{\text{eff}} = 0.14\,\text{m}^2/\text{s}$. The phase angles of the model coincide well with the measured phase angles; the absolute values of the model, however, do not match well with the measurements, although the model qualitatively predicts a similar slope for the decay of the transport transfer function's magnitude with respect to the frequency.

Note that the magnitude of the modeled transport function in Figure 11 does not approach unity for $St_t = 0$. This is due to the cooling of the combustor walls, which results in a smaller mean temperature (which is used for normalization) at measurement planes further downstream. This effect is included in the model by means of an empirical factor (≈ 0.88).

The considerable quantitative deviations that are observed in Figure 11 might not only be caused by the scattering of the data due to measurement uncertainties. To gain a better understanding of these discrepancies, the relevant parameters leading to the decay of the transport transfer function need to be identified.

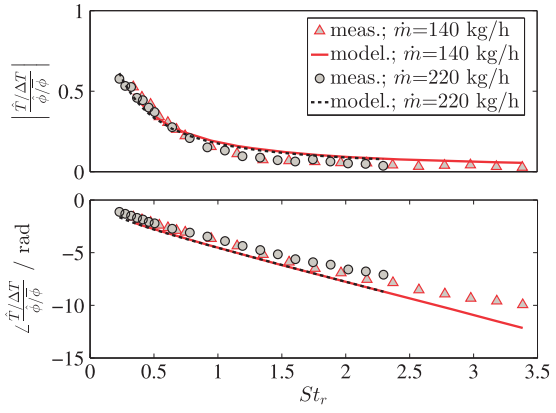

Figure 10. Absolute value (top) and phase (bottom) of the measured (solid) and modeled (dashed) reactor transfer function $\hat{H}_r$ for different mass flows $\dot{m} = 140$ kg/h (red) and $\dot{m} = 220$ kg/h (black); $\tau_r = 55$ ms; $\Delta x = 0.4$ m.

Table 2. Reactor model output parameters.

$\dot{m}$ (kg/h)	τ_r (ms)	$\bar{u}_r = (\Delta x_1/\tau_r)$ (m/s)	$\tilde{u}_r$ (m/s)
140	75	5.3	5.6
180	61	6.55	7.2
220	55	7.3	8.5

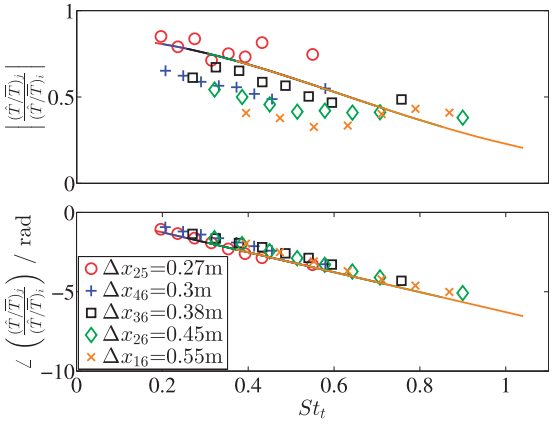

Figure 11. Absolute value (top) and phase (bottom) of the measured (marker) and modeled (line) transport transfer function $\hat{H}_t$ for different convection lengths Δx_{ij} (colors) and an air mass flow of $\dot{m} = 220$ kg/h; $Pe = 30$.

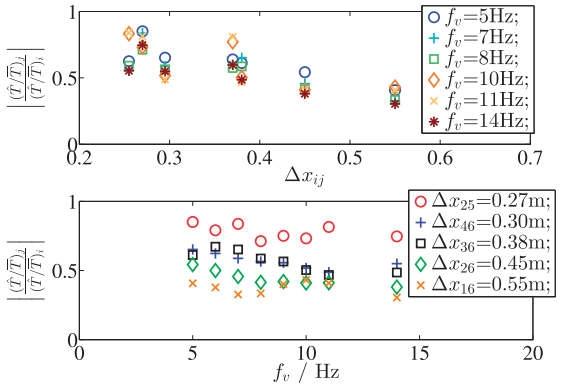

Figure 12. Measured absolute values of the transport transfer function with respect to the Δx_{ij} (top) and with respect to f_v (bottom); air mass flow $\dot{m} = 220$ kg/h.

Therefore, in Figure 12, the absolute values of the transport transfer functions are plotted for different frequencies with respect to the convective lengths (top) and for different transport distances with respect to the fuel modulation frequency (bottom). The attenuation of the normalized temperature amplitude clearly originates primarily from the transport length, whereas the frequency does not significantly affect the magnitude of the oscillations. The magnitudes of the normalized temperature fluctuations appear to be constant within the considered frequency range.

One reason might be the relatively small frequency range considered in this work. The lower frequency limit of 5 Hz is due to the flame dynamics, as below that limit, the flame strongly moves axially, leading to occasional extinction and reignition. For frequencies higher than $\approx$20 Hz, the amplitudes of the temperature fluctuations at the measurement planes further downstream are too small.

5. Conclusion

The goal of this study was to model the generation and the transport of entropy waves based on the experimental data. Dynamic temperature measurements were conducted at various axial locations downstream of a lean-premixed swirl-stabilized flame, which emitted entropy oscillations due to periodic modulation of the fuel supply.

A linearized well-stirred reactor model was derived, providing the transfer function between the equivalence ratio fluctuations upstream of the flame and the temperature fluctuations emerging from the exit of the reactor. Good agreement is found between the modeled normalized temperature fluctuations and the measured temperature fluctuations at the measurement plane closest to the flame. The low-pass character of the magnitude of the temperature perturbations is correctly reproduced, the unknown parameter in the model, the reactor residence time, is found to be of the order of the convective time scale obtained from the average bulk flow velocity. Hence, the reactor model enables a reliable prediction of the entropy fluctuations generated by a flame, provided that the equivalence ratio fluctuation is known.

For the analysis of the advective transport of an entropy wave from the reactor to positions further downstream, a convection–diffusion model is employed. Qualitatively, for the transfer function between temperature fluctuations at one measurement plane and the temperature fluctuations at a further upstream location, the model provides similar values as the measurements. Considerable quantitative deviations between the magnitudes of the fitted transport model and the measurements, however, require further experimental investigations.

Acknowledgements

The investigations were conducted as part of the joint research programme AG Turbo 2020 in the frame of AG Turbo. The authors gratefully acknowledge AG Turbo and GE Power for their support and permission to publish this paper. The responsibility for the content lies solely with its authors.

Declaration of Conflicting Interests

The author(s) declared no potential conflicts of interest with respect to the research, authorship, and/or publication of this article.

Funding

The author(s) disclosed receipt of the following financial support for the research, authorship, and/or publication of this article: The work was supported by the Bundesministerium für Wirtschaft und Technologie (BMWi) as per resolution of the German Federal Parliament under grant number 03ET2012P.

References

1. Polifke W, Paschereit CO and Döbbeling K. Constructive and destructive interference of acoustic and entropy waves in a premixed combustor with a choked exit. *Int J Acoust Vib* 2001; 6: 135–146.
2. Hubbard S and Dowling A. Acoustic instabilities in premix burners. In: *AIAA/CEAS, Aeroacoustics conference*, Toulouse, France, 1998.
3. Morgans AS and Duran I. Entropy noise: A review of theory, progress and challenges. *Int J Spray Combust Dyn* 2016, DOI: 10.1177/1756827716651791.
4. Bohn M. *Noise produced by the interaction of acoustic waves and entropy waves with high-speed nozzle flows*. PhD Thesis, California Institute of Technology, USA, 1976.

5. Marble F and Candel S. Acoustic disturbance from gas non-uniformities convected through a nozzle. *J Sound Vib* 1977; 55: 225–243.
6. Leyko M, Nicoud F and Poinsot T. Comparison of direct and indirect combustion noise mechanisms in a model combustor. *AIAA J* 2009; 47: 2709–2716.
7. Duran I and Moreau S. Solution of the quasi-one-dimensional linearized Euler equations using flow invariants and the Magnus expansion. *J Fluid Mech* 2013; 723: 190–231.
8. Zukoski E and Auerbach J. Experiments concerning the response of supersonic nozzles to fluctuating inlet conditions. *J Eng Power* 1976; 98: 60–64.
9. Bake F, Michel U and Röhle I. Investigation of entropy noise in aero-engine combustors. *J Eng Gas Turbines Power* 2007; 129: 370–376.
10. Dowling AP and Stow SR. Acoustic analysis of gas turbine combustors. *J Propul Power* 2003; 19: 751–764.
11. Strobio Chen L, Bomberg S and Polifke W. Propagation and generation of acoustic and entropy waves across a moving flame front. *Combust Flame* 2016; 166: 170–180.
12. Lieuwen T and Zinn B. The role of equivalence ratio oscillations in driving combustion instabilities in low NOx gas turbines. In: *27th symposium on combustion*, 1998, pp. 1809–1816. Pittsburg, PA: The Combustion Institute.
13. Sattelmayer T. Influence of the combustor aerodynamics on combustion instabilities from equivalence ratio fluctuations. *J Eng Gas Turbines Power* 2002; 125: 11–19.
14. Polifke W, Kopitz J and Serbanovic A. Impact of the fuel time lag distribution in elliptical premix nozzles on combustion stability. In: *7th AIAA/CEAS aeroacoustics conference and exhibit*, Maastricht, The Netherlands, 2001.
15. Schuermans B, Bellucci V, Guethe F, et al. A detailed analysis of thermoacoustic interaction mechanisms in a turbulent premixed flame. In: *Proceedings of ASME turbo expo 2004: Power for land, sea, and air*, Vienna, Austria, 2004.
16. Morgans AS, Goh CS and Dahan JA. The dissipation and shear dispersion of entropy waves in combustor thermoacoustics. *J Fluid Mech* 2013. DOI: 733. 10.1017/jfm.2013.448.
17. Goh C and Morgans A. The influence of entropy waves on the thermoacoustic stability of a model combustor. *Combust Sci Technol* 2013; 185: 249–268.
18. Dowling AP and Mahmoudi Y. Combustion noise. *Proc Combust Inst* 2015; 35: 65–100.
19. Kleppe J, Sanchez J and Fralick G. The application of acoustic pyrometry to gas turbines and jet engines. In: *Joint propulsion conferences*. Reston, VA: American Institute of Aeronautics and Astronautics, 1998.
20. DeSilva U, Bunce R and Claussen H. Novel gas turbine exhaust temperature measurement system. In: *ASME turbo expo*, San Antonio, USA, 2013.
21. Shen GQ, An LS and Jiang GS. Real-time monitoring on boiler combustion based on acoustic measurement. In: *2006 IEEE power India conference*, New Delhi, India, 2006, p. 4.
22. Golub GH and Loan CFV. *Matrix computations*, 3rd ed. Baltimore, MD: Johns Hopkins University Press, 1996.
23. Wassmer D, Schuermans B, Paschereit CO, et al. An acoustic time-of-flight approach for unsteady temperature measurements: Characterization of entropy waves in a model gas turbine combustor. *J Eng Gas Turbines Power* 2016; 139. DOI: 139. 10.1115/1.4034542.
24. Li H, Wehe SD and McManus KR. Real-time equivalence ratio measurements in gas turbine combustors with a near-infrared diode laser sensor. *Proc Combust Inst* 2011; 33: 717–724.
25. Blümner R, Ćosić B, Paschereit CO, et al. Experimental analysis of high-amplitude temporal equivalence ratio oscillations in the mixing section of a swirl-stabilized burner. In: *Proceedings of ASME turbo expo 2016*, Seoul, South Korea, GT2016-56585, p. 10.
26. Lieuwen T, Neumeier Y and Zinn BT. The role of unmixedness and chemical kinetics in driving combustion instabilities in lean premixed combustors. *Combust Sci Technol* 1998; 135: 193–211.
27. Karimi N, Brear MJ and Moase WH. Acoustic and disturbance energy analysis of a flow with heat communication. *J Fluid Mech* 2008; 597: 67–89.
28. Bobusch BC, Ćosić B, Moeck JP, et al. Optical measurement of local and global transfer functions for equivalence ratio fluctuations in a turbulent swirl flame. *J Eng Gas Turbines Power* 2013; 136: 021506–021506.
29. Taylor G. The dispersion of matter in turbulent flow through a pipe. *Proc R Soc Lond A Math Phys Sci* 1954; 223: 446–468.